Hydrolysis–Dehydration of Cellulose: Efficiency of NbZr Catalysts under Batch and Flow Conditions

Nikolay V. Gromov [1,*], Olga L. Ogorodnikova [1], Tatiana B. Medvedeva [1], Valentina N. Panchenko [1], Irina S. Yakovleva [1], Lyubov A. Isupova [1], Maria N. Timofeeva [1], Oxana P. Taran [1], Cyril Aymonier [2] and Valentin N. Parmon [1]

[1] Boreskov Institute of Catalysis SB RAS, Lavrentiev av. 5, 630090 Novosibirsk, Russia; parmon@catalysis.ru (V.N.P.)
[2] CNRS, University of Bordeaux, Bordeaux INP, ICMCB UMR5026, 33600 Pessac, France
[*] Correspondence: gromov@catalysis.ru; Tel.: +7-383-32-69-591

Abstract: Niobium oxide supported on ZrO_2 and mixed oxide of NbO_x-ZrO_2 was prepared and characterized. Mechanical treatment was followed by the microwave heating procedure of catalysts with more advanced textural parameters. The amount of Lewis (LAS) and Brønsted (BAS) acid sites rose with the increasing Nb content in the catalysts. The catalytic properties of samples of niobia-zirconia (NbZr samples, NbZr catalysts) were studied in a cellulose hydrolysis–dehydration reaction at 453 K under an inert Ar atmosphere in a batch reactor. Glucose and 5-hydroxumethylfurfural (5-HMF) were the major products. The initial reaction rate could be tuned by the density of acid sites on the surface of solid. At a low density of acid sites (0.1–0.3 $\mu mol \cdot m^{-2}$), the initial reaction rate had a pronounced inverse correlation. Increasing the LAS/BAS from 0.3 to 2.5 slightly stimulated the formation of the target products. The catalytic properties of NbZr catalysts prepared by microwave treatment were studied in cellulose transformation in a flow set-up. Glucose was found to be the major product. The maximum yield of glucose was observed in the presence of the sample of $17\%Nb/ZrO_2$. Increasing Nb content resulted in the formation of Nb-associated acid centers and, in turn, increasing catalyst acidity and activity.

Keywords: cellulose; hydrolysis–dehydration; glucose; 5-hydroxymethylfurfural; niobium oxide; zirconium oxide; batch reactor; flow reactor

1. Introduction

A promising alternative to limited fossils is a plant biomass which could provide a sustainable development based on renewable biobased raw materials [1,2]. Cellulose, being the most abundant inedible plant source, is a perspective renewable for the production of energy and chemicals [3,4]. The main product of cellulose hydrolysis is glucose, which is a substrate for the production of valuable chemicals such as formic acid [5–8], 5-hydroxymathylfurfural (5-HMF) [9], and sorbitol [10]. Notably, 5-HMF seems to be a perspective sleeping-platform bioorganic molecule and could be applied as a substrate for the synthesis of chemicals, biofuels, pharmaceuticals, plastics, etc. [11]. Thus, 2,5-dimethylfuran and 2-methylfuran, which are promising biofuels and octane booster additives, could be synthesized starting with 5-HMF. Compounds of 2,5-furandicarboxylic and 5-hydroxymethylfuranoic acids are also furan derivatives of 5-HMF with high potential in the fuel and polymer industries [12]. Moreover, 5-hydroxymethylfurfural is a precursor of non-furan derivatives, namely levulinic and adipic acids, 1,6-hexanediol, caprolactam, caprolactone, etc. [9].

It is known that the synthesis of 5-HMF from cellulose proceeds through three successive stages: (1) the hydrolysis of cellulose to glucose, (2) the isomerization of glucose to fructose, and then (3) the dehydration of fructose to 5-HMF. All the stages can be produced

in a one vessel (one-pot process) without the isolation and purification of the reaction intermediates, glucose and fructose (Scheme 1) [9,13,14].
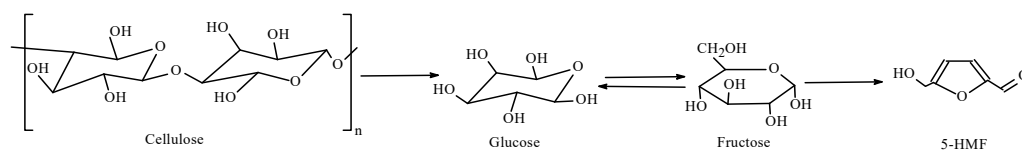
Scheme 1. One-pot synthesis of 5-HMF from cellulose.

However, direct processing the polysaccharide to 5-HMF is quite challenging as cellulose is insoluble in water and has a crystal structure. According to the literature, solid catalytic systems of heterogeneous catalysis present a perspective approach for the transformation of bioresources to valuable chemicals [1]. Heteropoly compounds [15], carbon materials [16], polymer resins, noble metal nanoparticles, and zeolites [17] can be used for the processing cellulose into 5-HMF. Water-insoluble oxides (ZrO_2, TiO_2, SiO_2, Nb_2O_5, etc.) are of particular interest for cellulose processing [18]. The high potential of zirconia catalysts in hydrolysis of cellulose was reported previously [19,20]. Recently, Yang et al. reported a 30% yield of reducing sugars of cellulose over zirconium oxide impregnated by SO_4^{2-} and supported on montmorillonite [21]. Catalysts based on niobium oxide can effectively dehydrate monosaccharaides to 5-HMF. Thus, Ngee et al. reported an 88% yield of 5-HMF from fructose over sulfated niobium oxide at 393 K in the presence of a DMSO co-solvent [22].

Materials based on niobium and zirconium oxides are of considerable interest in the processing of cellulose into 5-HMF due to the existing acid-base sites [19] and their high stability in hot water [23–26]. We previously investigated [27,28] one-pot hydrolysis–dehydration of mechanically activated cellulose in pure hot water to produce glucose and 5-hydroxymethylfurfural in the presence of amorphous niobium oxide supported on a zirconium dioxide (NbO_x/ZrO_2). It was found that activity of NbO_x/ZrO_2 systems depended on the Nb_2O_5 content and decreased as follows: $2.8\%Nb/ZrO_2{\sim}1.1\%Nb/ZrO_2 \gg ZrO_2 > 0.5\%Nb/ZrO_2$. The authors explained the trend by the changing aggregation state of niobium oxide species that led to the variation of the acid-base properties of the Nb/ZrO_2 composite. The highest glucose and 5-HMF yields (22 and 16 mol%, respectively) were obtained over $2.8\%Nb/ZrO_2$.

The nature of acidic sites is an important parameter for one-pot cellulose transformation processes. As reported previously, the isomerization of glucose to fructose proceeds on Lewis acid sites (LAS), while Brønsted acid sites (BAS) are responsible for hydrolysis and dehydration [26,29]. According to Nijhuis et al. [30], a maximum 55% yield of 5-HMF in the dehydration of glucose over titanium, zirconium, and niobium phosphate catalysts was observed at a BAS/LAS ratio of about 1. The catalytic properties of Nb/WO_3 also can be tuned by the variation of the BAS/LAS ratio. According to Yue et al. [24], a maximum 38% yield of 5-HMF was observed at a BAS/LAS ratio of 1.5. Thus, the design of catalytic materials with a high water tolerance and a suitable ratio of BAS/LAS is a challenge. Note that to our knowledge, an influence of the BAS/LAS ratio of NbO_x/ZrO_2 catalysts in cellulose hydrolysis–dehydration has not been reported previously.

A type of catalytic reactor can also affect the one-pot transformation of polysaccharides. Cellulose transformation is usually realized in batch reactors (autoclaves) in pure water. However, a flow reactor also can be used. Thus, fructose, sucrose, and inulin were dehydrated in the presence of phosphate-containing niobium catalysts under both batch and flow reactors [31]. It was demonstrated that a 51.2% conversion of fructose with a 59.4% selectivity of 5-HMF were achieved in a batch reactor at 373 K after 3 h, while a 45.5% conversion of fructose and a 58.0% selectivity of 5-HMF were achieved in a flow reactor at 358 K. The conversion of mono- and disaccharides to 5-HMF in the presence of catalysts based on niobium under flow conditions was investigated by Carniti et al. [26,32–34]. They demonstrated that the conversion of fructose and selectivity of 5-HMF were 68% and 34%,

respectively, in the presence of niobium phosphate at 373 K [34]. At the same, the transformation of cellobiose (disaccharide) at 403 K made it possible to achieve 5-HMF in 21% yield (31% selectivity, 70% substrate conversion) [26]. To our knowledge, the conversion of cellulose in the presence of solid oxide NbO_x and/or ZrO_2 catalytic systems in a flow reactor has not been carried out.

This work presents data on the evaluation of the influence of the BAS/LAS ratio and acid site density of Nb/ZrO_2 catalysts and on the possibility of using the catalysts under study to obtain glucose and 5-HMF under hydrothermal batch and flow conditions. We also aimed to reveal that an aggregation state of niobium oxide or acid properties of catalysts would be a key parameter which affects the catalyst activity.

2. Results

2.1. Synthesis and Characterization of Catalysts

Catalysts of niobium and zirconium oxides (also referred to as NbZr catalysts, NbZr samples, NbZr materials) were prepared two ways (Table 1). Such approach allowed us to reveal the effects of the agglomeration of the niobia particles, surface acidity, and ratio of Brønsted acid sites (BAS) and Lewis acid sites (LAS) (BAS/LAS ratio) on the reaction rate and selectivity toward 5-HMF in the one-pot hydrolysis–dehydration of cellulose.

Table 1. Textural characteristics of the NbZr catalysts.

№	Catalyst	Nb Content (wt.%)	Textural Properties				Phase Composition [1]	
			S_{BET} $(m^2 \cdot g^{-1})$	V_Σ $(cm^3 \cdot g^{-1})$	V_μ $(cm^3 \cdot g^{-1})$	D_{pore} (nm)	ZrO_2	Nb_xO_y
			Niobium oxide supported on ZrO_2 (NbZr-MAW)					
1	NbZr-MAW0	0	10	0.39	0.0009	86.6	M + T	A
2	NbZr-MAW1	0.6	49	0.83	0.0010	61.3	M + T	A
3	NbZr-MAW2	1.2	51	0.72	0.0014	48.9	M + T	A
4	NbZr-MAW3	6	60	0.49	0.0013	25.0	M + T	A
			Mixed oxide of NbO_x-ZrO_2 (NbZr-W)					
5	NbZr-W0	0	134	0.37	n.d.	9.5	A	A
6	NbZr-W1	2	221	0.49	n.d.	7.1	A	A
7	NbZr-W2	4	194	0.40	n.d.	7.3	A	A
8	NbZr-W3	17	154	0.72	n.d.	22.5	A	A

[1] M—monoclinic phase, T—tetragonal phase, A—amorphous phase.

Structural properties. First of all, we investigated structure of NbZr catalysts. X-ray diffraction patterns (XRD) of the samples are shown in Figure 1. It was found that the method of catalyst preparation affected the structure of ZrO_2. In XRD patterns of NbZr-MAW samples, we revealed characteristic diffraction peaks of monoclinic phase of ZrO_2 at diffraction angles (2Θ) 24.4°, 28.1°, 31.4°, 34.1°, 35.2°, 41.1°, 44.8°, 49.2°, and 50° (m-ZrO_2, JCPDS cards no. 37-1484) [35]. Moreover, the four peaks at 30.2, 35.2, 50.4, and 60.0° belonged to the tetragonal phase of ZrO_2 (t-ZrO_2, JCPDS cards no. 17-0923) [35]. Analysis of the XRD patterns of NbZr-W pointed to the amorphous phase for both ZrO_2 and Nb_2O_5 (Table 1). These results agree with the textural properties of NbZr materials.

Textural properties. The specific surface areas (S_{BET}) of the NbZr materials were calculated from the nitrogen adsorption isotherms using the Brunauer–Emmett–Teller (BET) method. The main results are shown in Table 1. As can be observed, the Nb content affected the textural properties of the NbZr-MAW materials. The increase in Nb content from 0 to 6 wt.% led to an increase in the specific surface area from 10 to 60 $m^2 \cdot g^{-1}$. At the same, the mean pore size changed in the reverse order. Note that NbZr-MAW0 and NbZr-MAW1 were macroporous solids, while NbZr-MAW2 and NbZr-MAW3 were mesoporous solids.
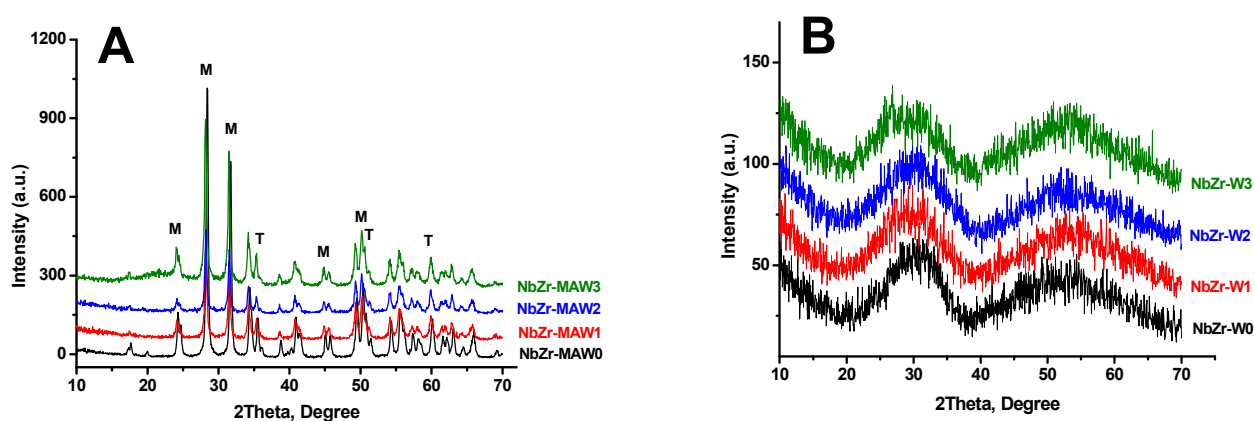
Figure 1. X-ray diffraction patterns of the NbZr-catalysts: (**A**)—NbZr-MAW and (**B**)—NbZr-W.

The specific surface area of the NbZr-W materials was higher in comparison with that of the NbZr-MAW samples; this can be explained by the difference in phase state (Table 1). The specific surface area also depends on the Nb content. The specific surface area rose with the increase in Nb loading. Moreover, all NbZr-W samples were mesoporous solids. The total pore volume does not change substantially when the Nb content increased from 0 to 4 wt.%, and the total pore content increased 1.8 times at 17 wt.% of Nb content in the sample.

It can be seen that synthesis via mechanical treatment and microwave heating makes it possible to obtain macro-/mesoporous materials. At the same time, mesoporous materials with high specific surface area can be obtained by the method of the joint microwave heating of niobia and zirconia precursors. Previously, we reported textural data on pure ZrO_2 samples [36]. It was found that oxide catalysts prepared by microwave heating, similar to the present work, had a higher specific surface area compared to catalysts produced by a combination of mechanical activation and microwave.

Electronic properties. The effect of method preparation and Nb content on the electronic properties of NbZr samples was investigated by Ultraviolet–visible diffuse reflectance spectroscopy (DR-UV-Vis). DR-UV-Vis spectra of NbZr samples are shown in Figures S1 and S2 (Supplementary Materials). The broad absorption in the 250–400 nm region associated with $O^{2-} \rightarrow Nb^{5+}$ charge transfer transition was observed in the spectrum of Nb_2O_5 [37]. The DR-UV-Vis spectra of all NbZr samples also contained this band. This band shifted to lower energy with the increase in the niobium content, indicating that Nb^{5+} and Zr^{4+} ions were electronically dependent.

The optical band edge can be discussed in the Tauc's equation related to the determination of band energy (E_g) (Equation (1)):

$$(\alpha h\nu)^{1/2} = B \cdot (h\nu - E_g) \tag{1}$$

where α is the absorbance, $h\nu$ is photon energy, B is an independent parameter of the photon's energy for the respective transitions, and E_g is the band gap. The plot of $(\alpha h\nu)^{1/2}$ versus $h\nu$ are displayed in Figures S1 and S2 (Supplementary Materials) for NbZr samples. The E_g values were determined from the steep absorption edge. The findings show that the E_g value for the studied NbZr samples depended on the Zr/Nb ratio and decreased with the increasing Nb content (Figure 2). A similar trend was demonstrated for a ZrO_2/Nb_2O_5 composite [38]. E_g values of the samples with $ZrO_2:Nb_2O_5$ mole ratios from 150:1 to 4:1 (from 1.3 to 33.5 mol % of Nb) decreased linearly with the Nb content [38]. This phenomenon was explained by the formation of the niobium oxide phase and changing oligomeric state of its particles.
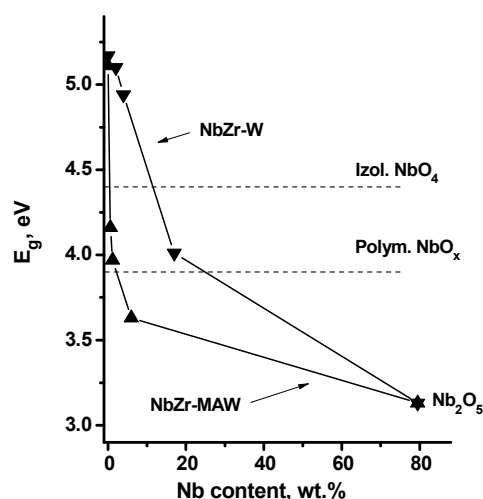
Figure 2. Influence of Nb content on a band gap (E_g).

The E_g values of 4.45 eV for niobium oxalate [39] and Nb-MCM-41 samples [40] corresponded to the predominant formation of isolated NbO_4 structures on the surface. E_g values equal to 3.9 eV were assigned to polymeric NbO_x structures, for example, to niobic acid Nb_2O_5 nH_2O [39]. According to that, NbO_x polymer structures on the surface of NbZr-MAW catalysts were formed in all synthesized samples containing 0.6, 1.2, and 6 wt. % of niobium (Figure 2). The catalysts of mixed oxides NbZr-W with a niobium content of 2 and 4 wt.% had isolated NbO_4 on the surface. The NbO_x polymer structures (E_g = 4.0 eV) were formed only on the surface of the NbZr-W3 sample which contained 17 wt % of Nb. Although increasing the red shift corresponded to rising the degree of polymerization of the NbO_x structures, the formation of bulk niobium oxide Nb_2O_5 (E_g = 3.42–3.2 eV [41]) was not observed for all the catalysts.

Nature of acid sites. The nature of active sites was investigated by IR spectroscopy. IR spectra of NbZr-MAW2 and NbZr-MAW3 samples preliminarily dehydroxylated at 673 K are shown in Figure S3 (Supplementary Materials). The spectrum of the NbZr-MAW2 sample contained a broad band with a maximum of 3600 cm^{-1} and, on its shoulder, a weak band around 3660 cm^{-1}, which can be assigned to the terminal and bridging –OH groups, respectively. At the same time, the intensity of the band at 3660 cm^{-1} was higher in comparison with that of the band at 3600 cm^{-1} in the spectrum of NbZr-MAW3. We can assume that this difference arose from the higher Nb content in NbZr-MAW3 (6 wt.%) than in NbZr-MAW2 (1.2 wt.%) that may have favored the appearance of hydrogen-bonded –OH groups.

The number and strength of acid sites in NbZr samples was analyzed by IR spectroscopy using pyridine as the probe molecule Figure S4 (Supplementary Materials). The main results are presented in Table 2. From, these data, the NbZr-W and NbZr-MAW samples contained both LAS and BAS on the surface. The number of acid sites also depended on the Nb content. Thus, the amount of LAS and BAS rose with the increasing Nb content in the NbZr-MAW samples prepared via mechanical treatment/microwave heating. The change of the molar ratio of LAS/BAS had a similar trend. However, for NbZr-W samples prepared via the joint microwave heating of niobia and zirconia precursors, the quantity of niobium had a small effect on the number of LAS and BAS and LAS/BAS molar ratio (Table 2).

The method of preparation of the NbZr samples affected the strength of the acid sites. The strength of the acid sites of the NbZr-W samples was higher (pH_{susp} 2.1–2.4) than that of NbZr-MAW (pH_{susp} 5.7–8.2) (Table 3). We suggest that this was due to the different ordering of the materials, as indicated by the XRD data.

Table 2. The BAS and LAS concentrations and BAS strength in the NbZr-W, NbZr-MAW, and Nb_2O_5 samples.

No	Catalyst Sample	Nb Content (wt.%)	BAS [1] ($\mu mol\ g^{-1}$)	LAS [2] ($\mu mol\ g^{-1}$)	Σ(LAS + BAS) ($\mu mol\ g^{-1}$)	LAS/BAS	ρ_{AS} [3] ($\mu mol \cdot m^{-2}$)
			NbZr-MAW samples				
1	NbZr-MAW0	0	n.d.	14	14	n/d	1.4
2	NbZr-MAW1	0.6	11	13	23	0.28	0.28
3	NbZr-MAW2	1.2	21	14	35	0.68	0.68
4	NbZr-MAW3	6.0	23	28	51	1.20	0.85
			NbZr-W samples				
5	NbZr-W0	0	n/d	n/d	n/d	n/d	0
6	NbZr-W1	2	10	22	32	2.18	0.14
7	NbZr-W2	4	6	13	19	2.16	0.10
8	NbZr-W3	17	10	24	34	2.5	0.22
9	Nb_2O_5	-	63	109	172	1.74	n/d

[1] Amount of BAS; [2] Amount of LAS; [3] Density of acid sites on the surface of solid (BAS + LAS)/S_{BET}, $\mu mol \cdot m^{-2}$.

Table 3. Cellulose conversion, yields of glucose and 5-HMF and initial reaction rate of cellulose hydrolysis-dehydration [1].

No	Catalyst	Nb Content (wt.%)	pH_{susp}	Conversion of Cellulose (%)	Yield			R [2] ($mmol \cdot L^{-1} \cdot h^{-1}$)
					Glucose	5-HMF	Other [3]	
				NbZr-MAW samples				
1	NbZr-MAW0	0	5.8	36	7.3	9.4	19.3	1.6
2	NbZr-MAW1	0.6	8.2	41	13.8	11.3	15.9	3.1
3	NbZr-MAW2	1.2	7.8	40	14.0	11.7	14.3	3.1
4	NbZr-MAW3	6.0	5.7	39	14.0	13.0	12.0	3.5
				NbZr-W samples				
5	NbZr-W0	0	2.2	50	17.5	12.5	20.0	7.5
6	NbZr-W1	2	2.1	51	16.9	12.5	21.6	8.4
7	NbZr-W2	4	2.2	37	14.7	11.5	10.8	8.4
8	NbZr-W3	17	2.4	41	15.6	12.9	12.5	4.7

[1] Experimental conditions: 10 g L^{-1} of cellulose in 45 mL of reaction mixture, 1 g L^{-1} of catalyst for NbZr-W samples and 0.5 g L^{-1} catalyst for NbZr-MAW samples, 1 MPa of Ar, 453 K, 7 h. [2] Initial rate of formation of target products (glucose + 5-HMF). [3] Cellobiose, fructose, furfural, acetic, formic, malic, levulinic, lactic, glycolic, and tartaric acids were detected.

2.2. Catalytic Properties of NbZr Catalysts in a Batch Reactor

The catalytic properties of NbZr catalysts were investigated in a cellulose hydrolysis–dehydration reaction at 10 g L^{-1} of cellulose in 45 mL of reaction mixture under an Ar atmosphere (1 MPa), 453 K, for 7 h. First of all, it was found that reaction in the presence of all studied NbZr catalysts was heterogeneous, following the hydrothermal stability tests of the NbZr catalysts. According to ICP-AES analysis, only 10^{-4}–10^{-3} wt.% of Nb and Zr were leached form solids.

Second, the analysis of reaction mixtures by HPLC shows that glucose and 5-HMF were the major products. Moreover, cellobiose, fructose, furfural, acetic, formic, malic, levulinic, lactic, glycolic, and tartaric acids were registered. The main results are shown in Table 4.

Effect of catalyst loading. The effect of catalyst content in the reaction mixture was investigated in the presence of NbZr-W3 and NbZr-MAW3. Correlations between the weight ratio of catalyst/cellulose and the yield of products are shown in Figure 3. One can see that the yield of glucose and 5-HMF depended on the cellulose/catalyst ratio. Thus, the total yield of glucose and 5-HMF did not exceed 40% of all products produced at an NbZr-W3/cellulose ratio of 1. Their total yield rose to 70% when the NbZr-W3/cellulose

was increased to 5 (Figure 3A). Note that the glucose/5-HMF ratio increased with the decreasing amount of catalyst.
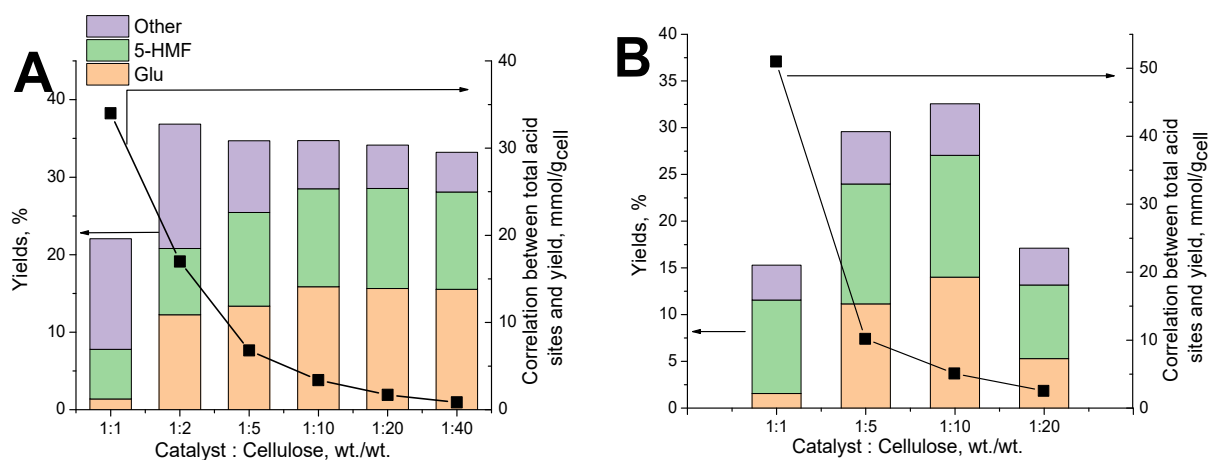
Figure 3. Correlation between the yield of products and the weight ratio of catalyst/cellulose. (**A**) NbZr-W3, (**B**) NbZr-MAW3. (Experimental conditions: 10 g L^{-1} of cellulose in 45 mL of reaction mixture, 1 MPa of Ar, 453 K, 7 h).

In the presence of NbZr-MAW3, the yield of the major products similarly depended on the catalyst loading (Figure 3B). Thus, when the NbZr-MAW3/cellulose ratio was 1/1, the yields of glucose and 5-HMF were 2 and 10%, respectively. The yield of glucose and 5-HMF increased to 14 and 13%, respectively, when decreasing the catalyst loading to 1 g L^{-1} (NbZr-MAW3/cellulose ratio = 1/10).

The changes in the total yield of major products and glucose/5-HMF ratio were caused by a decrease in the number of active centers available for the reaction. It should be noted that the subsequent transformations of the formed target reaction products to the side products and humins were catalyzed by the same active sites as the desired reactions. The optimum ratio of catalyst/cellulose made it possible to find a balance between the formation of glucose and 5-HMF and their degradation. Note that the efficiencies of NbZr-W3 and NbZr-MAW3 were different due to the different specific surface area and concentrations of active centers of NbZr-W3 and NbZr-MAW3 (Tables 1 and 2). Thus, the NbZr-W3 sample had an S$_{BET}$ of 154 m^2 g^{-1} and a total number of acid sites of 33.4 μmol g^{-1}, while the specific surface area of NbZr-MAW3 was 60 m^2 g^{-1} with an acid site concentration of 51.2 μmol g^{-1} (Table 2). According to the findings, the high yields of glucose and 5-HMF in the presence of NbZr-W and NbZr-MAW can be obtained at catalyst/cellulose weight ratio of 1/20 and 1/10, respectively.

Effect of acidity. The acidity of catalysts is a key parameter which determines catalyst activity [26,29,42,43]. A thorough analysis of the data showed no direct relationship between the catalytic activity of NbZr catalysts and the total amount of LAS and BAS (Figure S5, Supplementary Materials). Thus, we compared NbZr-MAW2 and NbZr-MAW3 (Table 4, lines 3 and 4). The catalysts had similar amounts of BAS and S$_{BET}$ (51–60 m^2 g^{-1}) and differed from each other in the LAS content by two times (NbZr-MAW3 > NbZr-MAW2). In the presence of both catalysts, the glucose yield was equals to 14%, while the 5-HMF yield and their initial reaction rate) were close. A similar result was found for the NbZr-W series.

It was reported previously that BAS centers are responsible for the hydrolysis of cellulose to glucose and dehydration of sugars to 5-HMF. On the other hand, LAS plays an important role in the isomerization of glucose to fructose (Scheme 1) [44]. Thus, it could be proposed that an appropriate combination of BAS and LAS could stimulate the reaction. However, during the investigation, the effect of the LAS/BAS ratio on the yields of glucose and 5-HMF was negligible. As can be seen from Figure 4A, the increase in the LAS/BAS ratio yield of major products did not increase significantly. However, according to [44],

increasing of LAS ratio favors the formation of the target products. Since catalysts have different textural characteristics, it can be assumed that their activity should be determined by the density of acid sites on the surface of NbZr samples. The correlation between the initial reaction rate (R) and the density of acid sites (ρ_{AS}) is shown in Figure 4B.
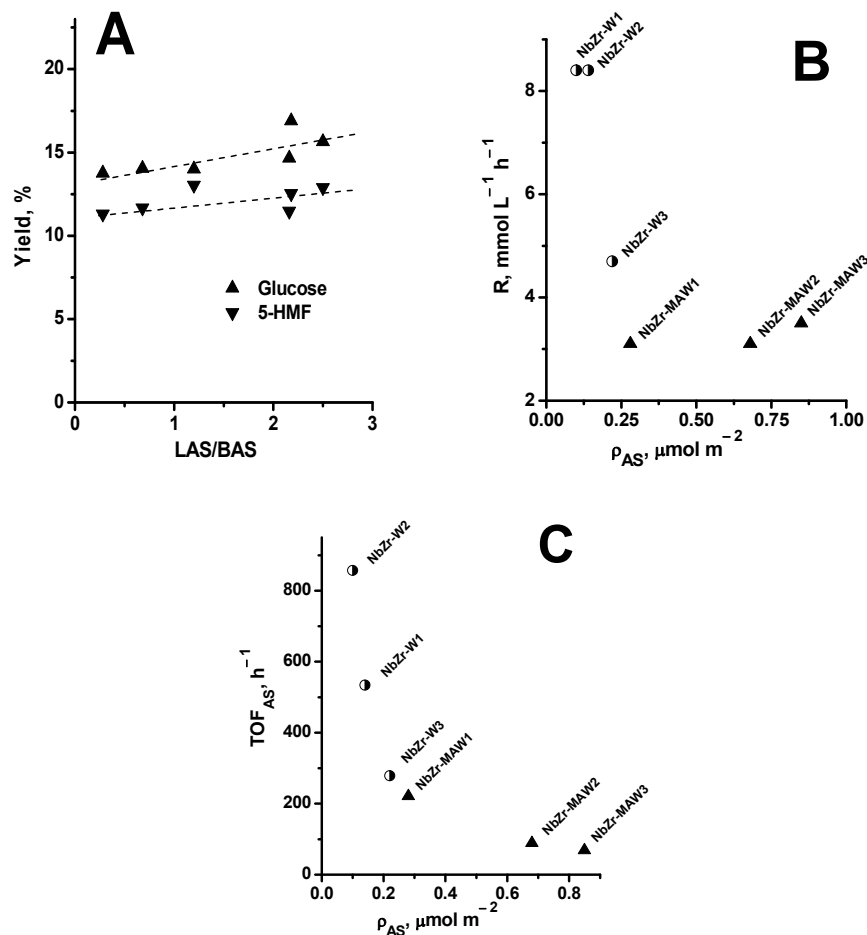
Figure 4. (**A**) Correlation between the yields of glucose and 5-HMF and the LAS/BAS ratio. (**B**) Correlation between the initial reaction rate and the density of acid sites. (**C**) Correlation between the TOF_{AS} and the density of acid sites.

It is clearly seen that the density of acid sites on the surface of the solid is an important parameter affecting the activity of NbZr samples. Two concentration areas can be distinguished: a low density of acid sites (0.1–0.3 μmol·m^{-2}) (region I) and a high density of acid sites (>0.3 μmol·m^{-2}) (region II). In the first region, the initial reaction rate decreased with the increasing density of acid sites, while in the second region, the effect of ρ_{AS} was negligible.

Since the samples had a different amount of acid sites, we estimated the efficiency of the NbZr catalyst using Equation (2):

$$TOF_{AS} = \frac{R}{m_{cat} \cdot [AS]} \tag{2}$$

where *R*—initial reaction rate (mmol·L^{-1}·h^{-1}); m_{cat}—amount of catalyst loaded (g); and [*AS*]—concentration of acid sites in a catalyst (mol g^{-1}).

The data shown in Figure 4C suggest that increasing the density of acid sites led to the decreasing activity of one active site. This trend can be the result of a decrease in the accessibility of the active site for reagents. Interestingly, the density of acid sites, not the aggregation of niobium, is a key parameter that significantly adjusted the catalyst activity.

Thus, NbZr-W2 was more active compared to NbZr-W1 (Figure 4C), although both catalysts contained isolated Nb structures (Figure 2).

Interestingly, the strength of acidic centers influenced the catalytic activity of the Nb-Zr oxide catalysts. Thus, NbZr-W1 had stronger acid sites (pH_{susp} 2.2) compared to NbZr-MAW1 (pH_{susp} 8.2) (Table 3). As a result, the activity (*R*) of NbZr-W1 was higher (8.4 mmol·L^{-1}·h^{-1}) in comparison with NbZr-MAW1 (3.1 mmol·L^{-1}·h^{-1}) (Table 2). Yields of glycose and 5-HMF were also higher in the presence of NbZr-W1 (16.9 and 12.5%, respectively) than that in the presence of NBZr-MAW1 (13.8 and 11.3%, respectively) (Table 3).

2.3. Catalytic Properties of NbZr Catalysts in a Flow Reactor

We were also interested in understanding the one-pot hydrolysis–dehydration of cellulose in the presence of NbZr catalysts in a flow set-up. This is because the majority of studies have focused on the studying the process in batch reactors. Thus, Sasaki et al. [45] investigated the transformation of microcrystalline cellulose under flow conditions at 563–673 K and 25 MPa. The authors reported 75% yields of different products (oligosaccharides, erythrose, dihydroxyacetone, fructose, glucose, glyceraldehyde).

Rogalinski et al. [46,47] studied cellulose transformation under both batch and flow modes and lower temperature of 483–583 K. The yields of glucose and its destruction products reached 5 and 10%, respectively, while the cellulose conversion was 25%. It was demonstrated that application of solid catalysts made it possible to decrease the reaction temperature. Overall, 75 and 10% yields of glucose and 5-HMF, respectively, were achieved when transforming microcrystalline cellulose at 473 K and 25 MPa pressure in the presence of Sibunit carbon materials treated to increase its acidity prior to the reaction [16].

Herein, we investigated the catalytic behavior of NbZr catalysts prepared by microwave treatment in a flow set-up. The series was chosen as it demonstrated high activity under batch conditions. According to the analysis of reaction mixtures by HPLC, glucose was the major product of the reaction. Moreover, reaction mixture contained water soluble oligosaccharides, cellobiose, glucose, fructose, 5-HMF, and furfural.

Effect of catalyst loading. The effect of catalyst loading on the reaction rate and yield of glucose was studied in the presence of NbZr-W2. The weight ratios of the NbZr-W2/cellulose were 1:1, 1:2.5, 1:5, and 1:10. Kinetic curves of glucose formation are shown in Figure 5A. These data reveal that the highest yield of glucose of 21% was observed when the catalyst/substrate ratio was 1/5. The decreasing of catalyst loading caused a simultaneous decrease in the glucose yield due to an insufficient number of active centers in the reactor. On the other hand, when the cellulose/catalyst ratio was 1/1(2.5), a decrease in the glucose yield was observed due to the significant transformation of glucose to side products.

Effect of Nb content. The effect of Nb content in NbZr catalyst on the yield of glucose was investigated in the presence of NbZr-W samples. The experiments were carried out at 473 K, a pressure of 25 MPa, a cellulose/catalyst ratio of 1/5, and a stop of water flow of 20 min. Kinetic curves of glucose accumulation are shown in Figure 5B. In the presence of zirconium oxide not promoted by NbO$_x$, a 20% yield of glucose was detected. Interestingly, the major product yield decreased to 13% when 2% of niobium was in the NbZr-W1 catalyst. Subsequently, glucose yields rose to 21 and 26% when Nb amount was 4 and 17%, respectively. (Figure 5B).

A similar trend of product yields on the niobium content we reported previously for cellulose processing in a batch reactor [27]. Decreasing activity of the catalyst, which had a minor Nb amount, accounted for the formation of isolated structures of Nb. Increasing the Nb content resulted in the formation of Nb-associated acid centers and, in turn, increased catalyst acidity. Thus, among the catalysts under study, NbZr-W3 catalyst was the most perspective, and a glucose yield of 26% was reached.
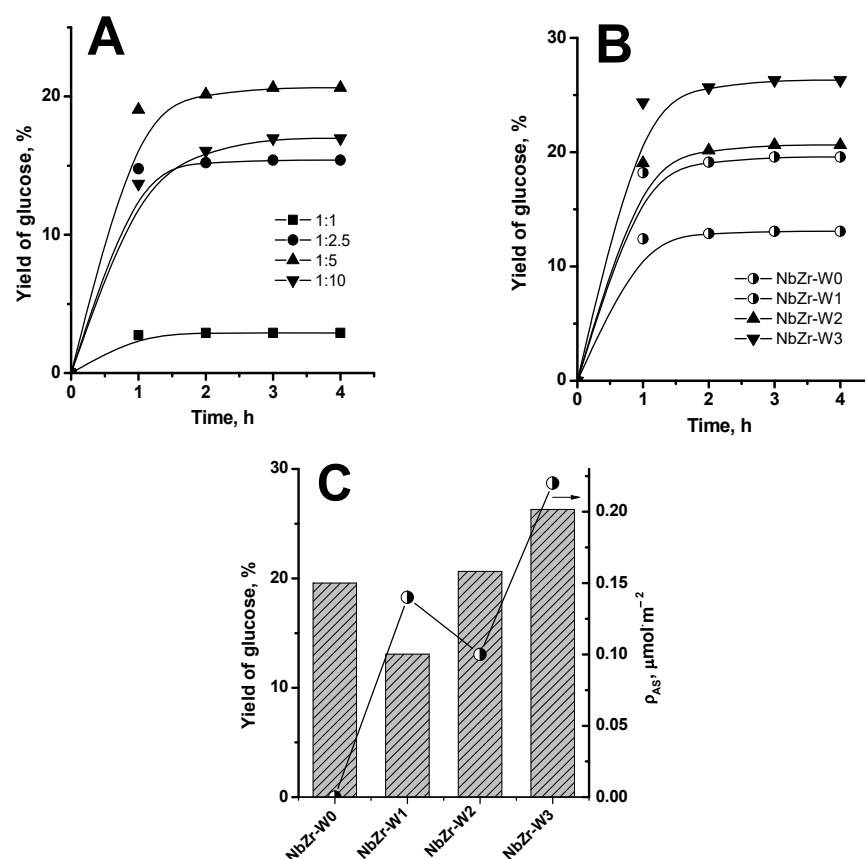
Figure 5. (**A**) Kinetic curves of glucose yield at different NbZr-W2/cellulose ratios in the cellulose hydrolysis–dehydration under flow conditions. (**B**) Kinetic curves of glucose yield at different Nb contents in the NbZr-W catalysts in the cellulose hydrolysis–dehydration under flow conditions. (**C**) Correlations between Nb content in the NbZr-W samples and the yield of glucose for 4 h and the density of acid sites on the surface of NbZr-W catalysts (ρ_{AS}). (Experimental conditions: 473 K, water pressure pump 20 MPa, stop flow, 20 min.).

2.4. Efficiency of NbZr Catalysts

It is interesting to compare the activity of oxide catalysts reported elsewhere with the one in this study. Table 4 summarizes the data on one-pot cellulose hydrolysis–dehydration to glucose and 5-HMF carried out in a batch reactor. As all the catalytic samples had different textural properties, we compared their activity estimated as *TOF* (Equation (3)):

$$TOF = \frac{R}{m_{cat}} \tag{3}$$

where *R*—initial reaction rate (mmol L^{-1} h^{-1}), and m_{cat}—amount of catalyst loaded (g).

The efficiency of NbZr-W2 (4% Nb) (Table 4, line 21) was higher in comparison with all studied catalytic materials. Chareonlimkun et al. [43] studied the activity of oxide catalysts TiO$_2$, ZrO$_2$, and TiO$_2$–ZrO$_2$ in the hydrolysis–dehydration of lignocellulose biomass. The most perspective catalysts were ZrO$_2$ and mixed TiO$_2$–ZrO$_2$. *TOFs* values of TiO$_2$–ZrO$_2$ and ZrO$_2$ were 13.9 and 7.6 mmol$_{5\text{-}HMF+Glu}$·g^{-1}·h^{-1}, respectively (Table 4, lines 3 and 5). The catalytic activity of Al$_2$O$_3$, SiO$_2$, ZnO–ZrO$_2$, ZrO$_2$-SO$_3$H, SiO$_2$-SO$_3$H, and Fe$_3$O$_4$-SiO$_2$-SO$_3$H was lower than NbZr-W2 [48–52]. In general, the efficiency of NbZr-MAW1 (0.6% Nb) was lower than that of ZrO$_2$, TiO$_2$–ZrO$_2$, and ZrO$_2$-SO$_3$; however, its efficiency was 8–10 times-higher higher compared to the efficiencies of systems of the similar composition (Table 4, lines, 20, 1, and 2).

Table 4. Catalytic properties of the heterogeneous catalysts in the transformation of cellulose via hydrolysis–dehydration in pure water.

№	Catalyst	T [1] (K)	Cell:H$_2$O:Cat [1] (g:mL:g)	Yield of 5-HMF (%)	*TOF* [1] (mmol g^{-1}·h^{-1})	Ref.
1	0.5% NbO$_x$/ZrO$_2$	453	1:100:1	12.9	0.4	[27]
2	2.8% NbO$_x$/ZrO$_2$	453	1:100:1	16.1	1.6	[27]
3	ZrO$_2$	523	1:10:1	8.2	7.6	[43]
4	TiO$_2$	523	1:10:1	10.0	13.0	[43]
5	TiO$_2$-ZrO$_2$	523	1:10:1	13.6	13.9	[43]
6	γ-Al$_2$O$_3$	423	1:10:1	-	0.06 [2]	[52]
7	SiO$_2$	423	1:10:1	-	0.0 [2]	[52]
8	SiO$_2$-SO$_3$H	423	1:10:1	-	1.1 [2]	[52]
9	Fe$_3$O$_4$-SiO$_2$-SO$_3$H	423	1:10:1	-	0.5 [2]	[52]
10	ZrO$_2$	433	0.3:67:1	-	0.02 [2]	[18]
11	TiO$_2$	433	0.3:67:1	-	0.004 [2]	[18]
12	Al$_2$O$_3$	433	0.3:67:1	-	0.002 [2]	[18]
13	SiO$_2$	433	0.3:67:1	-	0.09 [2]	[18]
14	ZnO-ZrO$_2$	463	1:100:1	5.8	0.09	[50]
15	SO$_4^{2-}$-ZrO$_2$/montmorillonite	473	5:50:1	-	10 [2]	[21]
16	ZrO$_2$-SO$_3$H	453	4:250:1	8.4	4 × 10^{-5}	[53]
17	ZrO$_2$-SO$_3$H	423	0.9:100:1	-	0.03 [2]	[49]
18	SiO$_2$	453	20:2000:1	-	0.007 [2]	[49]
19	γ-Al$_2$O$_3$	453	10:2000:1	-	0.007 [2]	[49]
20	NbZr-W2 (4%)	453	20:2000:1	-	16.8	This work
21	NbZr-MAW1 (0.6%)	453	10:2000:1	-	3.1	This work

[1] abbreviations: temperature (T), cellulose (Cell), catalyst (Cat); turnover frequency (*TOF*); [2] turnover frequency calculated in mmol (Glu)·g^{-1}·h^{-1}. The work does not present data on the yields of 5-HMF.

3. Materials and Methods

3.1. Materials

D-glucose (Reahim, Moscow, Russia), D-fructose (Sigma-Aldrich, St. Louis, MO, USA), D-mannose (Sigma-Aldrich), cellobiose (Alfa Aesar, Haverhill, MA, USA), 5-hydroxymethylfurfural (5-HMF) (Sigma-Aldrich), and levulinic acid (Acros Organics, Geel, Belgium) were used as high-pressure liquid chromatography (HPLC) standards. Detailed information on HPLC standards is described in the Supplementary Materials. Zirconyl oxynitrate ZrO(NO$_3$)$_2$xH$_2$O (Acros Organics) and niobium oxalate Nb(HC$_2$O$_4$)$_5$xH$_2$O (Sigma Aldrich) were used for the synthesis of catalysts.

Microcrystalline cellulose (fraction < 0.10 mm, Vekton, Saint-Petersburg, Russia) was used as the substrate. Microcrystalline cellulose was activated in a planetary mill Pulverizette 5 (Fristch, Idar-Oberstein, Germany) according to the method described in our previous works [15,16,54]. The particle size of cellulose was 13 ± 6 μm. The crystallinity index (CI) was 35–55%.

Milli-Q water (Millipore, France) was used to prepare all catalysts and reaction solutions, and it was also applied for the production of the high-pressure liquid chromatography (HPLC) sulfuric acid eluent (a flow rate of 0.6 mL min^{-1}).

Synthesis of catalysts. Two series of catalysts were prepared (Table 5). The first type of catalyst was niobium oxide supported on ZrO$_2$ (NbZr-MAW). ZrO$_2$ was prepared by the thermo degradation of zirconium oxynitrate. Then, niobia was formed by the mechanical treatment and microwave heating of ZrO$_2$ impregnated by niobium oxalate. The second type of catalyst was a mixed oxide of NbO$_x$-ZrO$_2$ (NbZr-W) prepared via the joint microwave heating of niobia and zirconia precursors.

Table 5. Conditions for the synthesis of Nb-Zr catalysts.

Catalyst	Nb Content (wt.%)	Preparation Method
Niobium oxide supported on Nb/ZrO$_2$ (NbZr-MAW)		
NbZr-MAW0	0	Step 1. Preparation of ZrO$_2$ by thermal decomposition of ZrO(NO$_3$)$_2\cdot$5H$_2$O at
NbZr-MAW1	0.6	873 K for 4 h.
NbZr-MAW2	1.2	Step 2. Mechanical activation of ZrO$_2$ and Nb(HC$_2$O$_4$)$_5$ for 2 min.
NbZr-MAW3	6	Step 3. Microwave treatment for 30 min
Mixed oxide of Nb-ZrO$_2$ (NbZr-W)		
NbZr-W0	0	
NbZr-W1	2	Microwave treatment mixture of ZrO(NO$_3$)$_2$ and Nb(HC$_2$O$_4$)$_5$) for 30 min
NbZr-W2	4	
NbZr-W3	17	

3.2. Catalyst Characterization

Analyses of the Nb and Zr content in samples were carried out by inductively coupled plasma-atomic emission spectrometry (ICP-AES) using a Perkin-Elmer instrument OPTIMA 4300.

The porous structures of samples were determined by the adsorption of N$_2$ at 77 K using an ASAP 2020 Plus the Quantachrome Autosorb-iQ instrument proposed by Micromeritics. The specific surface area (S$_{BET}$) was calculated from the adsorption data using the maxima arrangement modification of the BET method over the relative pressure range between 0.05 and 0.20. The total pore volume (V$_\Sigma$) was evaluated at a p/p_0 of 0.99.

The diffraction images (XRD) were obtained with the use of a Bruker D8 Advabced diffractometer (Manheim, Germany) with a non-monochromate Cu Kα radiation (λ = 1.5418 A), focusing geometry θ-θ in the scanning mode within the range of angles from 3 to 75°, with a step of 0.05°.

Infrared (IR) spectra were recorded by Shimadzu FTIR-8300S spectrometer (Kyoto, Japan) with a DRS-8000 diffusion reflectance cell in the range of 400 and 6000 cm^{-1}. Spectra resolution was 4 cm^{-1}. All spectra are presented in the $F(R)$ Kubelka–Munk scale (Equation (4)):

$$F(R) = \frac{(1-R)^2}{2R} \tag{4}$$

where R is the reflection coefficient.

IR spectroscopy using pyridine as probe molecules was used for the analysis of surface acidity (Supplementary Materials, Section S2.3).

Ultraviolet–visible diffuse reflectance spectroscopy (DR-UV–Vis) spectra were recorded on a UV-2501 PC Shimadzu spectrometer with an IRS-250A accessory in the 190–900 nm range with a resolution of 2 nm on samples in powder form placed into a special cell for DR-UV–Vis measurement. BaSO$_4$ was used as the standard for measurements.

The water pH suspension (pH$_{susp}$) of the catalysts was determined as follows. A 10 mL vial with water was purged with Ar for 10 min, and then 100 mg of the catalyst was added to water and the vial was hermetically sealed. The suspension was stirred on a shaker. The pH of mixture was measured in certain time intervals until equilibrium was reached. The pH of the reaction solutions was measured with an Anion 4100 pH tester (TD Anion, Novosibirsk, Russia).

The total organic carbon balance (TOC) was measured by Multi N/C 2100S TOC Analyzer (Analytik Jena, Jena, Germany).

3.3. Catalytic Test in a Batch Reactor

Hydrothermal stability tests were carried out in a batch reactor (Autoclave Engineers, Erie, PA, USA) at 453 K, Ar pressure 1 MPa, and vigorous stirring 1000 rpm. To investigate catalyst stability, a catalyst (450 mg) and water (45 mL) were placed into the autoclave. The

stability test time was 3 h. Leaching of Zr and Nb after hydrothermal treatment was carried out by ICP-AES analysis.

Hydrolysis–dehydration of cellulose was investigated in the batch reactor first at 453 K under an argon atmosphere. High-pressure autoclave produced by Autoclave Engineers (USA) was used for the batch experiments. Initial cellulose loading was 10 g·L^{-1}. The amount of catalyst varied in the range of 0.25–10 g·L^{-1}. The volume of the reaction mixture was 45 mL.

Analysis of the reaction mixtures was carried out by HPLC. Shimadzu Prominence LC-20 apparatus was used. The chromatograph was equipped by a RI detector and Rezex ROA-Organic Acids column (Phenomenex, 300 × 5.0 mm, Torrance, CA, USA). Additional information on catalyst testing techniques can be found in our previous papers [27,36,55].

3.4. Catalytic Test in a Flow Reactor

Hydrolysis–dehydration of cellulose under flow conditions was carried out in a set-up equipped with a pump, back pressure regulator, and temperature controller [16]. The scheme of the apparatus of hydrolysis–dehydration of cellulose under flow conditions is presented in Figure S6 (Supplementary Materials). The reactor was a stainless-steel tube (length 200 mm, inner diameter 2.7 mm). The experiments were carried out at a temperature of 473 K and 25 MPa of water. The experiment time was 4 h. A typical experiment was carried out as follows. A mechanical mixture of a catalyst (25–250 mg) and cellulose (250 mg) was placed in the reactor. Pure water was pumped through a thermostated reactor at a rate of 0.5 mL·min^{-1}. The installation worked in the stop-flow mode. Water was pumped through the reactor for 40 min, then the flow was stopped for 20 min [16]. At the outlet of the reactor, the reaction mixture was cooled to room temperature and collected in separate flasks every hour for analysis of the reaction products.

Analysis of reaction mixtures to determine the content of glucose and other products of cellulose depolymerization was carried out by HPLC on an Ultimate 3000 Thermo Scientific ultrahigh pressure liquid chromatograph (UHPLC) (Waltham, MA, USA) equipped with a Shodex SH1011 (Showa Denco, Tokyo, Japan) column thermostated at 333 K and a RI detector. An aqueous solution of 5 mM H_2SO_4 was used as the eluent. The eluent flow rate was 0.6 mL·min^{-1}.

The yield of the products was calculated as follows (Equation (5)) [55]:

$$Y = \frac{V \cdot C_{product}}{N_{cellulose} \cdot \left(\frac{m_{cellulose}}{m_{glucan}} \right)} \cdot 100\% \tag{5}$$

where Y—a product yield (%), $C_{product}$—a product concentration (mol L^{-1}), V—reaction mixture volume (L), $m_{cellulose}$—cellulose loading (g), Nc—stoichiometric coefficient between a glucan unit and a product (1 for glucose and 5-HMF, 6 for formic acid etc.), and m_{glucan}—molar weight of glucan unit in cellulose (162 g mol^{-1}).

The initial reaction rate was calculated according to Equation (6):

$$R = \frac{(C_{Glu} + C_{5-HMF}) - (C_{Glu}^0 + C_{5-HMF}^0)}{t} \tag{6}$$

where R—initial reaction rate (mmol L^{-1} h^{-1}); C_{Glu} and C_{5-HMF}—concentration of glucose and 5-HMF (mmol L^{-1}), respectively, achieved at the second kinetic point (1h); C^0_{Glu} and C^0_{5-HMF}—concentration of glucose and 5-HMF (mmol L^{-1}), respectively, the first kinetic point; and t reaction time (h).

4. Conclusions

Herein, we prepared two NbZr series of catalysts. The first type of catalyst was a niobium oxide supported on ZrO_2 prepared by the thermo degradation of zirconium oxynitrate (NbZr-MAW). Niobia was formed on the surface by mechanical treatment and microwave heating. The second type of catalyst was a mixed oxide of NbO_x-ZrO_2 (NbZr-W) derived via the joint microwave heating of niobia and zirconia precursors. The catalysts were characterized by N_2 low-temperature adsorption; XRD, DR-UV–Vis, IR spectroscopy, and pH suspension was also determined.

The samples of NbZr-MAW had a low S_{BET} (10–60 m^2/g). On the other hand, mechanical treatment followed by microwave heating allowed us produce catalysts having more advanced textural parameters of 134–221 m^2 g^{-1}. DR-UV–Vis analysis of the catalysts and pure supports was carried out. The E_g values of the absorption edge of the catalysts depended on the content of niobium and the type of support. The catalysts of mixed oxides NbZr-W with a niobium content of 2 and 4 wt.% had isolated NbO_4 on the surface. NbO_x polymer structures were formed on the surface of the NbZr-W3 sample only, which contained 17 wt % of Nb. The nature of the acid sites was investigated by IR spectroscopy using pyridine as probe molecule. It was found that the amount of LAS and BAS rose with the increasing Nb content in NbZr samples.

Catalytic properties of NbZr samples were studied in the cellulose hydrolysis–dehydration reaction at 453 K under an inert Ar atmosphere in a batch reactor. The optimal catalyst/substrate ratios of 1/20 and 1/10 were determined for the NbZr-W and NbZr-MAW catalysts, respectively. The effect of total amount of acid sites on the reaction rate and yield of glucose and 5-HMF was negligible. However, it was found that increasing the LAS/BAS from 0.3 to 2.5 slightly stimulated the formation of the target products. At the same time, the initial reaction rate could be tuned by the density of acid sites on the surface of solid. At a low density of acid sites (0.1–0.3 $\mu mol \cdot m^{-2}$), the initial reaction rate had a pronounced inverse correlation. Further increasing the density of AS (>0.3 $\mu mol \cdot m^{-2}$) had a minor effect on the catalytic activity. The *TOF* values of the catalysts demonstrated correlations similar to ones of initial reaction rate. To our knowledge, the NbZr-W2 catalyst which contained 4% of Nb was more effective compared to the catalytic materials of similar composition described previously. We believe that it provides a high potential of the catalysts of Nb/ZrO_2 prepared by microwave treatment for the production of 5-HMF from cellulose polysaccharide.

The datalytic properties of NbZr-W catalysts also were determined in cellulose transformation in a flow set-up. Glucose was found to be the major product. Using NbZr-W2, the influence of catalyst loading on the process was investigated to reveal the optimum substrate/catalyst ratio. It was found that the highest yield of glucose of 21% was observed when catalyst/substrate ratio was 1/5. The effect of Nb content on the NbZr-W catalysts was demonstrated. It was found that maximal yield of glucose (26%) was observed in the presence of NbZr-W3 (17% Nb). It was suggested that decreasing activity of the catalyst which had a low Nb amount accounted for the formation of isolated structures of Nb. Increasing the Nb content resulted in the formation of Nb-associated acid centers and, in turn, increased catalyst acidity.

References

1. Tabassum, N.; Pothu, R.; Pattnaik, A.; Boddula, R.; Balla, P.; Gundeboyina, R.; Challa, P.; Rajesh, R.; Perugopu, V.; Mameda, N.; et al. Heterogeneous Catalysts for Conversion of Biodiesel-Waste Glycerol into High-Added-Value Chemicals. *Catalysts* **2022**, *12*, 767. [CrossRef]
2. Pothu, R.; Mameda, N.; Mitta, H.; Boddula, R.; Gundeboyina, R.; Perugopu, V.; Radwan, A.B.; Abdullah, A.M.; Al-Qahtani, N. High Dispersion of Platinum Nanoparticles over Functionalized Zirconia for Effective Transformation of Levulinic Acid to Alkyl Levulinate Biofuel Additives in the Vapor Phase. *J. Compos. Sci.* **2022**, *6*, 300. [CrossRef]
3. Delidovich, I.; Leonhard, K.; Palkovits, R. Cellulose and hemicellulose valorisation: An integrated challenge of catalysis and reaction engineering. *Energy Environ. Sci.* **2014**, *7*, 2803–2830. [CrossRef]
4. Gallezot, P. Conversion of biomass to selected chemical products. *Chem. Soc. Rev.* **2012**, *41*, 1538–1558. [CrossRef]
5. Gromov, N.V.; Medvedeva, T.B.; Rodikova, Y.A.; Babushkin, D.E.; Panchenko, V.N.; Timofeeva, M.N.; Zhizhina, E.G.; Taran, O.P.; Parmon, V.N. One-pot synthesis of formic acid via hydrolysis–oxidation of potato starch in the presence of cesium salts of heteropoly acid catalysts. *RSC Adv.* **2020**, *10*, 28856–28864. [CrossRef]
6. Gromov, N.V.; Medvedeva, T.B.; Sorokina, K.N.; Samoylova, Y.V.; Rodikova, Y.A.; Parmon, V.N. Direct Conversion of Microalgae Biomass to Formic Acid under an Air Atmosphere with Soluble and Solid Mo–V–P Heteropoly Acid Catalysts. *ACS Sustain. Chem. Eng.* **2020**, *8*, 18947–18956. [CrossRef]
7. Gromov, N.V.; Medvedeva, T.B.; Lukoyanov, I.A.; Panchenko, V.N.; Timofeeva, M.N.; Taran, O.P.; Parmon, V.N. Formic Acid Production via One-Pot Hydrolysis-Oxidation of Starch over Quaternary Ammonium Salts of Vanadium-Containing Keggin-Type Heteropoly Acids. *Catalysts* **2022**, *12*, 1252. [CrossRef]
8. Valentini, F.; Kozell, V.; Petrucci, C.; Marrocchi, A.; Gu, Y.; Gelman, D.; Vaccaro, L. Formic acid, a biomass-derived source of energy and hydrogen for biomass upgrading. *Energy Environ. Sci.* **2019**, *12*, 2646–2664. [CrossRef]
9. Van Putten, R.J.; van der Waal, J.C.; de Jong, E.; Rasrendra, C.B.; Heeres, H.J.; de Vries, J.G. Hydroxymethylfurfural, a versatile platform chemical made from renewable resources. *Chem. Rev.* **2013**, *113*, 1499–1597. [CrossRef]
10. Ribeiro, L.S.; Órfão, J.J.d.M.; Pereira, M.F.R. Direct catalytic production of sorbitol from waste cellulosic materials. *Bioresour. Technol.* **2017**, *232*, 152–158. [CrossRef]
11. Rout, P.K.; Nannaware, A.D.; Prakash, O.; Kalra, A.; Rajasekharan, R. Synthesis of hydroxymethylfurfural from cellulose using green processes: A promising biochemical and biofuel feedstock. *Chem. Eng. Sci.* **2016**, *142*, 318–346. [CrossRef]
12. Siankevich, S.; Savoglidis, G.; Fei, Z.; Laurenczy, G.; Alexander, D.T.L.; Yan, N.; Dyson, P.J. A novel platinum nanocatalyst for the oxidation of 5-Hydroxymethylfurfural into 2,5-Furandicarboxylic acid under mild conditions. *J. Catal.* **2014**, *315*, 67–74. [CrossRef]
13. Gallezot, P.; Kiennemann, A. Conversion of Biomass on Solid Catalysts. In *Handbook of Heterogeneous Catalysis*; Wiley: Weinheim, Germany, 2008; pp. 2447–2476. [CrossRef]
14. Bruggink, A.; Schoevaart, R.; Kieboom, T. Concepts of Nature in Organic Synthesis: Cascade Catalysis and Multistep Conversions in Concert. *Org. Process Res. Dev.* **2003**, *7*, 622–640. [CrossRef]
15. Gromov, N.V.; Medvedeva, T.B.; Taran, O.P.; Timofeeva, M.N.; Parmon, V.N. Hydrolysis of Cellulose in the Presence of Catalysts Based on Cesium Salts of Heteropoly Acids. *Catal. Ind.* **2021**, *13*, 73–80. [CrossRef]
16. Aymonier, C.; Gromov, N.V.; Taran, O.P.; Parmon, V.N. Hydrolysis–dehydration of cellulose to glucose and 5-hydroxymethylfurfural over Sibunit solid acid carbon catalysts under semi-flow conditions. *Wood Sci. Technol.* **2021**, *55*, 607–624. [CrossRef]

17. Nandiwale, K.Y.; Galande, N.D.; Thakur, P.; Sawant, S.D.; Zambre, V.P.; Bokade, V.V. One-Pot Synthesis of 5-Hydroxymethylfurfural by Cellulose Hydrolysis over Highly Active Bimodal Micro/Mesoporous H-ZSM-5 Catalyst. *ACS Sustain. Chem. Eng.* **2014**, *2*, 1928–1932. [CrossRef]

18. Wang, H.; Zhang, C.; He, H.; Wang, L. Glucose production from hydrolysis of cellulose over a novel silica catalyst under hydrothermal conditions. *J. Environ. Sci.* **2012**, *24*, 473–478. [CrossRef]

19. Wattanapaphawong, P.; Reubroycharoen, P.; Yamaguchi, A. Conversion of cellulose into lactic acid using zirconium oxide catalysts. *RSC Adv.* **2017**, *7*, 18561–18568. [CrossRef]

20. Joshi, S.S.; Zodge, A.D.; Pandare, K.V.; Kulkarni, B.D. Efficient Conversion of Cellulose to Levulinic Acid by Hydrothermal Treatment Using Zirconium Dioxide as a Recyclable Solid Acid Catalyst. *Ind. Eng. Chem. Res.* **2014**, *53*, 18796–18805. [CrossRef]

21. Yang, H.; Zhou, Y.; Tong, D.; Yang, M.; Fang, K.; Zhou, C.; Yu, W. Catalytic conversion of cellulose to reducing sugars over clay-based solid acid catalyst supported nanosized SO_4^{2-}-ZrO_2. *Appl. Clay Sci.* **2020**, *185*, 105376. [CrossRef]

22. Ngee, E.L.S.; Gao, Y.; Chen, X.; Lee, T.M.; Hu, Z.; Zhao, D.; Yan, N. Sulfated Mesoporous Niobium Oxide Catalyzed 5-Hydroxymethylfurfural Formation from Sugars. *Ind. Eng. Chem. Res.* **2014**, *53*, 14225–14233. [CrossRef]

23. Qiao, Y.; Feng, L.; Li, Z.; Zhang, Z.; Chen, J.; Na, H.; Zhu, J.; Chen, L. Effect of Adsorption of ZrO_2 in Catalysts on the Efficiency of Hydrolysisof Cellulose to Sugar in Aqueous System under Microwave Radiation. *Chin. J. Chem.* **2020**, *38*, 399–405. [CrossRef]

24. Yue, C.; Li, G.; Pidko, E.A.; Wiesfeld, J.J.; Rigutto, M.; Hensen, E.J.M. Dehydration of Glucose to 5-Hydroxymethylfurfural Using Nb-doped Tungstite. *ChemSusChem* **2016**, *9*, 2421–2429. [CrossRef]

25. Kreissl, H.T.; Nakagawa, K.; Peng, Y.-K.; Koito, Y.; Zheng, J.; Tsang, S.C.E. Niobium oxides: Correlation of acidity with structure and catalytic performance in sucrose conversion to 5-hydroxymethylfurfural. *J. Catal.* **2016**, *338*, 329–339. [CrossRef]

26. Carniti, P.; Gervasini, A.; Bossola, F.; Dal Santo, V. Cooperative action of Brønsted and Lewis acid sites of niobium phosphate catalysts for cellobiose conversion in water. *Appl. Catal. B Environ.* **2016**, *193*, 93–102. [CrossRef]

27. Gromov, N.V.; Taran, O.P.; Semeykina, V.S.; Danilova, I.G.; Pestunov, A.V.; Parkhomchuk, E.V.; Parmon, V.N. Solid Acidic NbOx/ZrO_2 Catalysts for Transformation of Cellulose to Glucose and 5-Hydroxymethylfurfural in Pure Hot Water. *Catal. Lett.* **2017**, *147*, 1485–1495. [CrossRef]

28. Gromov, N.V.; Yakovleva, I.S.; Isupova, L.A.; Parmon, V.N.; Taran, O.P. Solid acid catalysts based on niobium and zirconium oxides for hydrolysis-dehydration of cellulose into glucose and 5-hydroxymethylfurfural. Impact of preparation technique on catalytic properties. *J. Sib. Fed. Univ. Chem.* **2020**, *13*, 283–296. [CrossRef]

29. Zhang, Y.; Wang, J.; Li, X.; Liu, X.; Xia, Y.; Hu, B.; Lu, G.; Wang, Y. Direct conversion of biomass-derived carbohydrates to 5-hydroxymethylfurural over water-tolerant niobium-based catalysts. *Fuel* **2015**, *139*, 301–307. [CrossRef]

30. Ordomsky, V.V.; Sushkevich, V.L.; Schouten, J.C.; van der Schaaf, J.; Nijhuis, T.A. Glucose dehydration to 5-hydroxymethylfurfural over phosphate catalysts. *J. Catal.* **2013**, *300*, 37–46. [CrossRef]

31. Carlini, C.; Giuttari, M.; Maria Raspolli Galletti, A.; Sbrana, G.; Armaroli, T.; Busca, G. Selective saccharides dehydration to 5-hydroxymethyl-2-furaldehyde by heterogeneous niobium catalysts. *Appl. Catal. A Gen.* **1999**, *183*, 295–302. [CrossRef]

32. Marzo, M.; Gervasini, A.; Carniti, P. Hydrolysis of disaccharides over solid acid catalysts under green conditions. *Carbohydr. Res.* **2012**, *347*, 23–31. [CrossRef]

33. Carniti, P.; Gervasini, A.; Biella, S.; Auroux, A. Niobic acid and niobium phosphate as highly acidic viable catalysts in aqueous medium: Fructose dehydration reaction. *Catal. Today* **2006**, *118*, 373–378. [CrossRef]

34. Carniti, P.; Gervasini, A.; Biella, S.; Auroux, A. Intrinsic and Effective Acidity Study of Niobic Acid and Niobium Phosphate by a Multitechnique Approach. *Chem. Mater.* **2005**, *17*, 6128–6136. [CrossRef]

35. Ding, S.; Zhao, J.; Yu, Q. Effect of Zirconia Polymorph on Vapor-Phase Ketonization of Propionic Acid. *Catalysts* **2019**, *9*, 768. [CrossRef]

36. Medvedeva, T.B.; Ogorodnikova, O.L.; Yakovleva, I.S.; Isupova, L.A.; Taran, O.P.; Gromov, N.V.; Parmon, V.N. Impact of Design on the Activity of ZrO_2 Catalysts in Cellulose Hydrolysis-Dehydration to Glucose and 5-Hydroxymethylfurfural. *Catalysts* **2021**, *11*, 1359. [CrossRef]

37. Armaroli, T.; Busca, G.; Carlini, C.; Giuttari, M.; Raspolli Galletti, A.M.; Sbrana, G. Acid sites characterization of niobium phosphate catalysts and their activity in fructose dehydration to 5-hydroxymethyl-2-furaldehyde. *J. Mol. Catal. A Chem.* **2000**, *151*, 233–243. [CrossRef]

38. İlknur, Ç. Preparation and Characterization of Niobia-Containing Solid Acid. Ph.D. Thesis, Bilkent University, Ankara, Turkey, 2010.

39. Onfroy, T.; Clet, G.; Houalla, M. Correlations between Acidity, Surface Structure, and Catalytic Activity of Niobium Oxide Supported on Zirconia. *J. Phys. Chem. B* **2005**, *109*, 14588–14594. [CrossRef]

40. Gao, X.; Wachs, I.E.; Wong, M.S.; Ying, J.Y. Structural and Reactivity Properties of Nb-MCM-41: Comparison with That of Highly Dispersed Nb_2O_5/SiO_2 Catalysts. *J. Catal.* **2001**, *203*, 18–24. [CrossRef]

41. Shao, R.; Zeng, X.; Cao, Z.; Dong, H.; Wang, L.; Wang, F.; Liu, J.; Li, Z.; Liang, Q. A novel Ag_3PO_4/Nb_2O_5 fiber composite with enhanced photocatalytic performance and stability. *RSC Adv.* **2015**, *5*, 102101–102107. [CrossRef]

42. Watanabe, M.; Aizawa, Y.; Iida, T.; Nishimura, R.; Inomata, H. Catalytic glucose and fructose conversions with TiO_2 and ZrO_2 in water at 473K: Relationship between reactivity and acid–base property determined by TPD measurement. *Appl. Catal. A Gen.* **2005**, *295*, 150–156. [CrossRef]

43. Chareonlimkun, A.; Champreda, V.; Shotipruk, A.; Laosiripojana, N. Catalytic conversion of sugarcane bagasse, rice husk and corncob in the presence of TiO$_2$, ZrO$_2$ and mixed-oxide TiO$_2$–ZrO$_2$ under hot compressed water (HCW) condition. *Bioresour. Technol.* **2010**, *101*, 4179–4186. [CrossRef]

44. Hassan, N.S.; Jalil, A.A. Cellulose conversion into renewable chemicals and fuels over supported metal catalysts. *IOP Conf. Ser. Mater. Sci. Eng.* **2020**, *808*, 012002. [CrossRef]

45. Sasaki, M.; Kabyemela, B.; Malaluan, R.; Hirose, S.; Takeda, N.; Adschiri, T.; Arai, K. Cellulose hydrolysis in subcritical and supercritical water. *J. Supercrit. Fluids* **1998**, *13*, 261–268. [CrossRef]

46. Rogalinski, T.; Ingram, T.; Brunner, G. Hydrolysis of lignocellulosic biomass in water under elevated temperatures and pressures. *J. Supercrit. Fluids* **2008**, *47*, 54–63. [CrossRef]

47. Rogalinski, T.; Liu, K.; Albrecht, T.; Brunner, G. Hydrolysis kinetics of biopolymers in subcritical water. *J. Supercrit. Fluids* **2008**, *46*, 335–341. [CrossRef]

48. Dhepe, P.L.; Fukuoka, A. Cellulose Conversion under Heterogeneous Catalysis. *ChemSusChem* **2008**, *1*, 969–975. [CrossRef]

49. Onda, A.; Ochi, T.; Yanagisawa, K. Selective hydrolysis of cellulose into glucose over solid acid catalysts. *Green Chem.* **2008**, *10*, 1033–1037. [CrossRef]

50. Yang, F.; Li, G.; Gao, P.; Lv, X.-N.; Sun, X.; Liu, Z.-H.; Fan, H. Mild Hydrothermal Degradation of Cotton Cellulose by using a Mixed-Metal-Oxide ZnO–ZrO$_2$ Catalyst. *Energy Technol.* **2013**, *1*, 581–586. [CrossRef]

51. Gavilà, L.; Güell, E.J.; Maru, B.T.; Medina, F.; Constantí, M. Combining catalytical and biological processes to transform cellulose into high value-added products. *Phys. Sci. Rev.* **2017**, *2*, 26. [CrossRef]

52. Lai, D.-m.; Deng, L.; Li, J.; Liao, B.; Guo, Q.-x.; Fu, Y. Hydrolysis of Cellulose into Glucose by Magnetic Solid Acid. *ChemSusChem* **2011**, *4*, 55–58. [CrossRef]

53. Yatsenko, D.A.; Medvedeva, T.B. Estimating Crystality Index of Microcrystalline Cellulose Using Diffraction Methods. *J. Struct. Chem.* **2019**, *60*, 1430–1436. [CrossRef]

54. Gromov, N.V.; Medvedeva, T.B.; Taran, O.P.; Bukhtiyarov, A.V.; Aymonier, C.; Prosvirin, I.P.; Parmon, V.N. Hydrothermal Solubilization–Hydrolysis–Dehydration of Cellulose to Glucose and 5-Hydroxymethylfurfural Over Solid Acid Carbon Catalysts. *Top. Catal.* **2018**, *61*, 1912–1927. [CrossRef]

55. Gromov, N.V.; Taran, O.P.; Aymonier, C.; Parmon, V.N. Kinetic modeling of the multistep hydrolysis-dehydration of cellulose to platform molecules over a solid carbon acid catalyst in pure water. *React. Kinet. Mech. Catal.* **2020**, *130*, 669–684. [CrossRef]